

**Shape evolution in the superdeformed  $A \approx 80-90$  mass region**K. Lagergren,<sup>1</sup> B. Cederwall,<sup>1</sup> R. M. Clark,<sup>2</sup> P. Fallon,<sup>2</sup> A. Görgen,<sup>2,\*</sup> T. Issa,<sup>1</sup> R. V. F. Janssens,<sup>3</sup> A. Johnson,<sup>1</sup> A. O. Macchiavelli,<sup>2</sup> L. Milechina,<sup>1</sup> D. G. Sarantites,<sup>4</sup> and R. Wyss<sup>1</sup><sup>1</sup>*Department of Physics, Royal Institute of Technology, SE-10691 Stockholm, Sweden*<sup>2</sup>*Nuclear Science Division, Lawrence Berkeley National Laboratory, Berkeley, California 94720, USA*<sup>3</sup>*Physics Division, Argonne National Laboratory, Argonne, Illinois 60439, USA*<sup>4</sup>*Department of Chemistry, Washington University, St. Louis, Missouri 63130, USA*

(Received 27 July 2003; published 31 December 2003)

Superdeformed bands in  $^{88}\text{Mo}$ ,  $^{89}\text{Tc}$ , and  $^{91}\text{Tc}$  were populated using a  $^{40}\text{Ca}$  beam with an energy of 185 MeV, impinging on a backed  $^{58}\text{Ni}$  target.  $\gamma$  rays and charged particles emitted in the reactions were detected using the Gammasphere Ge detector array and the CsI(Tl) array Microball. Average transition quadrupole moments  $Q_t$ , with significantly improved accuracy compared to earlier work, were deduced for the bands using the residual doppler shift technique. The experimental results were included into a systematic study of the  $Q_t$  values throughout the superdeformed mass 80–90 region. The superdeformed shell gaps are predicted to move towards larger deformations with increasing  $Z$  and  $N$  in this mass region. This trend is confirmed by the experimental  $Q_t$  values.

DOI: 10.1103/PhysRevC.68.064309

PACS number(s): 21.10.Ky, 21.10.Re, 21.10.Tg, 27.50.+e

**I. INTRODUCTION**

Since the first discovery of a superdeformed (SD) band in the nucleus  $^{83}\text{Sr}$  by Baktash *et al.* [1], the  $A \approx 80-90$  mass region has revealed a rich spectroscopy of SD states. This mass region, which stands out compared to other SD regions in the nuclear chart due to its proximity to the proton drip line as well as to the  $N=Z$  line, is of special interest for several reasons. First, since protons and neutrons near the respective Fermi levels occupy identical or similar orbitals, constructive interference between the two fermion systems may enhance the stability of large deformations. This applies in particular to the nucleus  $^{88}\text{Ru}$ , with  $Z=N=44$ , which is predicted to be the “doubly magic” SD nucleus of the mass region, and to exhibit favored SD states even in the low-spin regime. Second, due to the proximity to the proton drip line, unbound proton “continuum” states are located close to the Fermi level and may affect the SD structures in new ways. This might lead to proton decay competing with the  $\gamma$  decay out of the SD states. A third special feature of this region of SD nuclei is that the ground states and low-lying states exhibit a shape change with decreasing deformation as a function of increasing mass, with relatively large deformations for the nuclei with lower masses and almost spherical shapes for the heavier nuclei in this region. The difference in deformation between SD and ND states is relatively modest for the Sr isotopes and increases when approaching the Tc and Mo isotopes in the heavier part of the mass region. This allows for the unique possibility to study the interplay between SD and ND states as a function of their relative deformation by studying the decay out of the SD bands. The results of such a systematic study will be presented elsewhere [2].

In this work we examine the shape evolution of SD states experimentally by means of Doppler shift measurements. The new improved experimental information includes data on the nuclei  $^{88}\text{Mo}$ ,  $^{89}\text{Tc}$ , and  $^{91}\text{Tc}$ .

**II. EXPERIMENTAL PROCEDURE**

The experiment was performed at the 88-inch cyclotron of the Lawrence Berkeley National Laboratory, using a 185-MeV  $^{40}\text{Ca}$  ion beam with an average intensity of  $\approx 4$  pA. The two different targets used in the experiment consisted of 0.35- and 0.32-mg/cm<sup>2</sup>  $^{58}\text{Ni}$ , enriched to 99.6%, on 1-mg/cm<sup>2</sup> gold backings. The targets were turned 10° from the beam axis in order to minimize the shadow effect of the target frame on the charged particle detectors.  $\gamma$  rays emitted in the reactions were detected using the Gammasphere Ge detector array [3], at the time of the experiment comprising 102 large escape-suppressed coaxial  $n$ -type high-purity Ge detectors. The targets were thin enough to allow fusion-evaporation products to recoil into the vacuum of the target chamber, and the emitted  $\gamma$  rays detected by Gammasphere were consequently Doppler shifted. The 46 detectors placed closest to 90° relative to the beam axis were electronically divided into two segments. The primary interaction points of the  $\gamma$  rays could therefore (on average) be determined with a higher accuracy for these detectors, improving the Doppler correction of the  $\gamma$  rays, and thereby the effective energy resolution in the spectra.

The event trigger applied in the data acquisition system required coincidences between five or more escape-suppressed Ge detectors. Approximately  $1.4 \times 10^9$  raw events were collected during 6 days of irradiation time and were stored on magnetic tapes for later offline analysis. The heavymet absorbers, which normally protect the BGO suppression shields from direct hits by  $\gamma$  rays from the reactions, were removed in order to enable the use of the detector system as a calorimeter. This information was used to improve the reaction channel selectivity [4,5].

---

\*Present address: DAPNIA/SPhN, CEA Saclay, F-91191 Gif-sur-Yvette Cedex, France.

The CsI(Tl) detector array Microball [6] was used in conjunction with Gammasphere to detect charged particles emitted from the compound nuclei, mainly protons and  $\alpha$  particles. The pulse shapes of the scintillation signals from the Microball detectors were used to determine the type of each detected particle. The efficiencies for detecting and correctly identifying an emitted particle were  $\approx 69\%$  and  $46\%$  for protons and  $\alpha$  particles, respectively. The emission of particles gives a significant contribution to the recoil of the nucleus, affecting the associated  $\gamma$ -ray energies in the laboratory system. This was corrected for using the particle identity and linear momentum information provided by the Microball, thus reducing the Doppler broadening of the  $\gamma$  lines in particle-gated spectra. The reaction channels studied in this work were  $^{88}\text{Mo}(2\alpha 2p)^{89}\text{Tc}(2\alpha 1p)$ , and  $^{91}\text{Tc}(1\alpha 3p)$ .

The data were sorted offline, and a search for new discrete SD structures was performed. This was done by applying sums of double gates while systematically varying the positions of and distances between the gates. This search resulted in the finding of one new SD band, which was assigned to  $^{88}\text{Mo}$  on the basis of coincidences with known lower-lying transitions [7]. This result is discussed elsewhere [8].

The residual Doppler shift technique [9] can be used to extract the lifetimes of SD states from thin-target data. These states have sufficiently short lifetimes to have a significant possibility to decay while the reaction product nucleus still remains inside even a thin target, and the mean velocity of the nuclei therefore varies as a function of the excitation energy in a SD band. The thicknesses of the two target layers used in the present experiment were optimized to slow down the product nuclei as quickly as possible during the decay of the SD bands, while still allowing the lower-lying states to decay in the vacuum of the target chamber after the recoiling nuclei have passed through the composite target. By the use of a backed target, a steeper (average) velocity dependence as a function of excitation energy in the SD bands than for normal homogenous targets was obtained, allowing for improved accuracy in the lifetime estimates for SD states. Mean velocity values for each SD configuration were obtained from the Doppler shifts of the  $\gamma$  rays. Average transition quadrupole moments  $Q_t$  for each SD band could be deduced by comparing the experimental velocity values to a simple rotational model using known stopping powers [10] and averaging over different production depths inside the fertile part of the target. Each band was assumed to be fed through a cascade of two transitions with  $B(E2)$  values similar to those of the superdeformed band, an assumption to which the final results are not very sensitive. The side feeding was modeled using transition intensities extracted from the experimental data. A  $\chi^2$  minimization procedure was applied to find the  $Q_t$  value for which the velocity curve most closely follows the experimental data points. Results for  $^{89}\text{Tc}$  and  $^{91}\text{Tc}$ , shown in Fig. 1, illustrate the procedure.

### III. EXPERIMENTAL RESULTS

The previously observed SD bands in  $^{88}\text{Mo}$  [11] (three bands),  $^{89}\text{Tc}$  [12] (one band), and  $^{91}\text{Tc}$  [13] (one band) were confirmed in this work. The transition energies were obtained

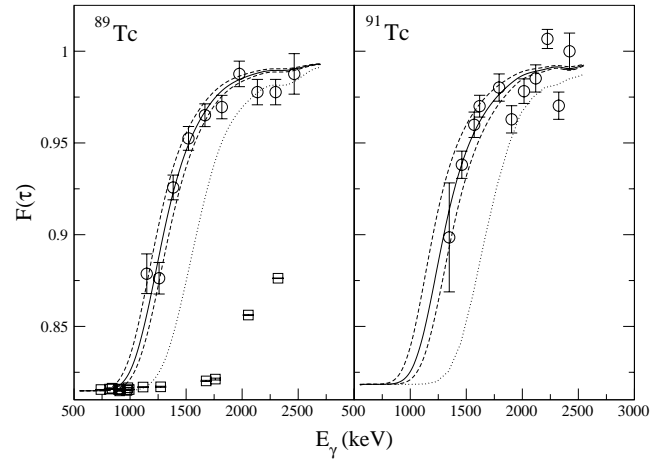


FIG. 1. Experimentally deduced fractional Doppler shifts  $F(\tau)$ , as a function of  $\gamma$ -ray energy for the SD bands assigned to  $^{89}\text{Tc}$  (left panel) and  $^{91}\text{Tc}$  (right panel) are indicated by the circles.  $F(\tau)$  is defined as the ratio between the average velocity that the nuclei have when emitting a certain  $\gamma$  ray and the average initial velocity of the nuclei. The velocity as a function of  $\gamma$ -ray energy was obtained from the residual Doppler shift of the  $\gamma$  rays after a partial Doppler correction (using a constant velocity as a function of energy) has been made. Transitions between known ND states in  $^{88}\text{Mo}$  are included for comparison (squares). The error bars show only the statistical uncertainties. For  $^{89}\text{Tc}$ , the solid line corresponds to  $Q_t = 5.9 e b$  and the dashed lines to  $Q_t = 5.6$  and  $6.6 e b$  (corresponding to the uncertainties given in Table II). For  $^{91}\text{Tc}$ , these values are  $Q_t = 6.7, 5.9,$  and  $8.0$ . The dotted line has been included for comparison and corresponds to  $Q_t = 3.5 e b$  in both cases.

with an improved accuracy. In addition, one new SD band was found and assigned to  $^{88}\text{Mo}$ . The transition energies for the SD bands assigned to the nuclei  $^{88}\text{Mo}$ ,  $^{89}\text{Tc}$ , and  $^{91}\text{Tc}$ , as deduced from the present work, are included in Table I. Spectra showing the SD bands in these nuclei are presented in Figs. 2–4. Previously reported [7,14,15]  $\gamma$ -ray transitions between lower-lying yrast states in each nucleus (corresponding to spherical shell model configurations) are marked

TABLE I. Transition energies for the SD bands observed in the present experiment. Statistical uncertainties are given within parentheses. The transition placed at the top of the SD band in  $^{89}\text{Tc}$  is tentative.

$^{89}\text{Tc}$	$^{91}\text{Tc}$	$^{88}\text{Mo}(1)$	$^{88}\text{Mo}(2)$
1149.2(3)	1348.4(3)	1238.6(4)	1459.6(8)
1258.83(11)	1459.51(4)	1342.07(23)	1595.6(7)
1384.35(7)	1569.75(17)	1480.70(23)	1743.1(5)
1521.18(8)	1681.97(13)	1633.45(22)	1894.8(5)
1668.09(6)	1792.63(13)	1795.50(25)	2054.2(9)
1818.82(8)	1903.79(16)	1962.2(3)	2224.3(16)
1974.57(9)	2014.84(17)	2133.4(5)	
2136.01(10)	2119.26(17)	2306.5(11)	
2298.34(13)	2224.13(27)		
2462.0(16)	2325.9(3)		
(2619(3))	2421.5(3)		

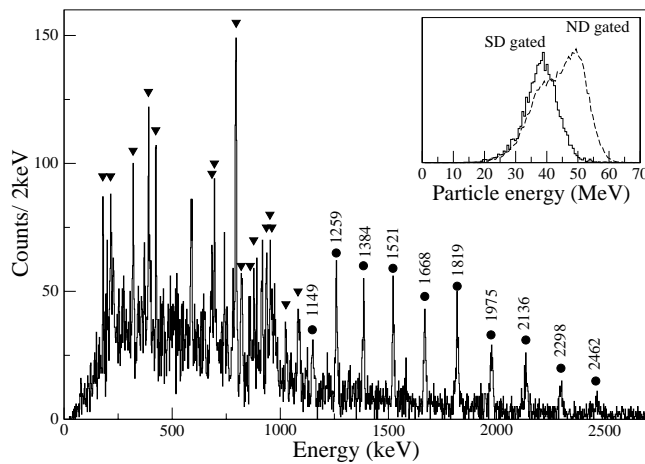


FIG. 2. Spectrum produced by summing all combinations of triple gates on the transitions of the SD band in  $^{89}\text{Tc}$  for events where two  $\alpha$  particles and one or zero protons were detected. A filter based on the total detected energy and the  $\gamma$  ray multiplicity has been applied to the data, and relevant background contributions have been subtracted. The inset compares spectra for the total energy of the charged particles detected in coincidence with transitions from the SD band (SD) and lower-lying transitions (ND). As expected, the average energy of the emitted charged particles is lower when the SD band is populated. The unusually strong relative intensity of the SD band in this nucleus reveals itself as the “bump” in the “ND” particle energy spectrum. Compare, e.g., with the same picture for  $^{91}\text{Tc}$  (see Fig. 3), where this feature is not present. Transitions assigned to the SD band are indicated by filled circles, and transitions between lower-lying states in the same nucleus are indicated by triangles.

in the spectra. The insets in Figs. 2 and 3 compare the energy distributions of the charged particles emitted in coincidence with the SD bands, with those emitted in coincidence with known lower-lying transitions. The average total energy of the detected charged particles is lower for events where the SD bands were populated, since the nuclei, on average, are populated at a higher excitation energy in this case. Also, note that the curve gated by the ND transitions has a different shape in the case of  $^{89}\text{Tc}$ . This is due to the remarkably high relative intensity (around 15%) of this SD band [12].

#### IV. DISCUSSION

The dynamical  $\mathcal{J}^{(2)}$  moments of inertia for the SD bands observed in the present experiment are plotted in Fig. 5, and the experimentally deduced  $Q_i$  values for bands 1 and 2 in  $^{88}\text{Mo}$  and the bands in  $^{89,91}\text{Tc}$  are included in Table II. The new  $Q_i$  values are consistent (within experimental error limits) with the previous work (in which  $Q_i$  was deduced as  $6.0_{-1.4}^{+2.0} e b$  for band 1 in  $^{88}\text{Mo}$  [11],  $6.7_{-2.3}^{+3.0} e b$  for the SD band in  $^{89}\text{Tc}$  [12], and  $8.1_{-1.4}^{+1.9} e b$  for  $^{91}\text{Tc}$  [13]). The  $Q_i$  value for  $^{91}\text{Tc}$  obtained in the present work is lower than expected for a purely prolate shape and the very large observed dynamical moment of inertia (see Fig. 5) that has been observed for this nucleus. The high  $\mathcal{J}^{(2)}$  values for this band was earlier [13] attributed to an unusually large, “enhanced” deformation. It is possible that the relatively low  $Q_i/\mathcal{J}^{(2)}$  ratio

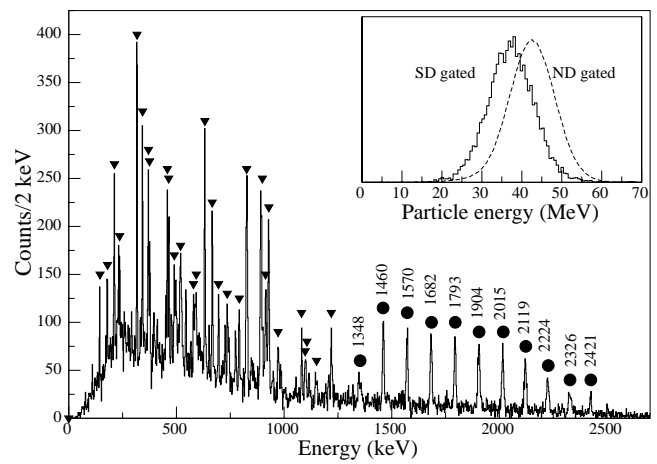


FIG. 3. Spectrum obtained by summing all combinations of triple gates on the transitions in the SD band in  $^{91}\text{Tc}$  in coincidence with  $1\alpha 3p$ ,  $1\alpha 2p$ , or  $1\alpha 1p$ , and subtracting a background spectrum. A gate criterion on the total detected energy and  $\gamma$ -ray multiplicity was also applied. In the inset the total energy distribution of the charged particles detected in coincidence with the SD band is compared with a distribution in coincidence with known lower-lying transitions in the same nucleus. Transitions connecting states in the SD band are marked by circles, and previously established transitions between lower-lying states are indicated by triangles.

is a consequence of  $^{91}\text{Tc}$  having a triaxial shape with a positive  $\gamma$  deformation parameter. In the limit of high angular momenta, pairing correlations are weakened and the moment of inertia approaches that of a rigid body. For positive values of the  $\gamma$  deformation parameter, this results in an increasing moment of inertia and in a decreasing transition quadrupole moment relative to an axially symmetric quadrupole shape.

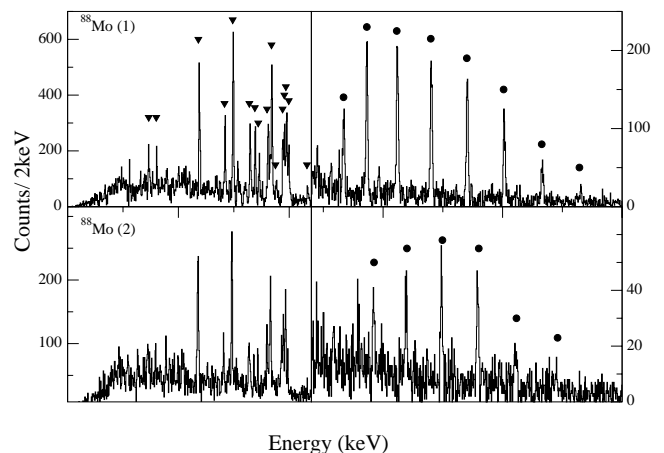


FIG. 4. Background subtracted spectra showing the SD bands (bands 1 and 2) of  $^{88}\text{Mo}$  discussed in this article. The spectra have been obtained by applying double gates on the in-band transitions. Two  $\alpha$  particles and one or two protons were required in coincidence with the  $\gamma$  rays. In addition, the events were subject to a simultaneous criterion applied to the total detected  $\gamma$ -ray multiplicity and total detected energy, in order to further filter out any contaminants emanating from other reaction channels. Transitions assigned to the SD bands are indicated by circles, and previously established lower-lying transitions by triangles.

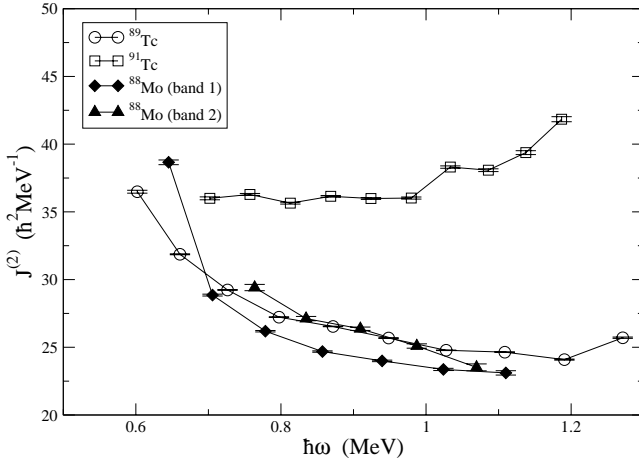


FIG. 5. Experimental dynamical  $\mathcal{J}^{(2)}$  moments of inertia for the SD bands discussed in this work plotted as a function of rotational frequency. Note the very high  $\mathcal{J}^{(2)}$  moment of inertia for the band assigned to  $^{91}\text{Tc}$  and the irregularity in the curve that may indicate a band crossing. Statistical uncertainties are indicated by the error bars.

TABLE II. Deduced  $Q_t$  values and assigned  $\mathcal{N}=5$  intruder orbital occupation numbers for the SD bands in the mass 80–90 region. The values in the second column have been plotted as a function of  $Z$  in Fig. 6.

SD band	$Q_t(\text{eb})$	Assignment	Ref.
$^{80}\text{Sr}(1)$	$3.42^{+0.26}_{-0.23}$	$\nu 5^1 \pi 5^0$	[22]
$^{80}\text{Sr}(2)$	$3.63^{+0.17}_{-0.15}$	$\nu 5^1 \pi 5^0$	[22]
$^{80}\text{Sr}(3)$	$4.1^{+0.6}_{-0.6}$	$(\nu 5^1 \pi 5^0)$	[22]
$^{80}\text{Sr}(4)$	$4.9^{+0.6}_{-0.6}$	$\nu 5^1 \pi 5^1$	[22]
$^{81}\text{Sr}(1)$	$3.08^{+0.16}_{-0.15}$	$\nu 5^1 \pi 5^0$	[22]
$^{81}\text{Sr}(2)$	$3.30^{+0.27}_{-0.21}$	$\nu 5^1 \pi 5^0$	[22]
$^{82}\text{Sr}$	$3.54^{+0.15}_{-0.14}$	$\nu 5^1 \pi 5^0$	[22]
$^{83}\text{Sr}$	$3.60^{+0.20}_{-0.18}$	$\nu 5^1 \pi 5^0$	[22]
$^{82}\text{Y}$	$4.3^{+1.8}_{-0.8}$	$\nu 5^1 \pi 5^0 / \nu 5^1 \pi 5^1$	[22]
$^{83}\text{Y}(1)$	$4.4^{+0.7}_{-0.7}$	$\nu 5^1 \pi 5^1$	[22]
$^{83}\text{Y}(2)$	$3.6^{+0.8}_{-0.5}$	$\nu 5^1 \pi 5^0$	[22]
$^{83}\text{Y}(3)$	$3.6^{+0.4}_{-0.3}$	$(\nu 5^0 \pi 5^0)$	[22]
$^{84}\text{Y}$	$3.6^{+0.5}_{-0.9}$	$\nu 5^1 \pi 5^0$	[22]
$^{83}\text{Zr}(1)$	$5.8^{+0.8}_{-0.5}$	$\nu 5^2 \pi 5^1$	[22]
$^{84}\text{Zr}$	$5.6^{+0.6}_{-0.5}$	$\nu 5^2 \pi 5^1$	[22]
$^{86}\text{Zr}(1)$	$4.6^{+0.7}_{-0.6}$	$\nu 5^2 \pi 5^1$	[23]
$^{86}\text{Zr}(2)$	$4.0^{+0.3}_{-0.3}$	$\nu 5^2 \pi 5^1$	[23]
$^{86}\text{Zr}(3)$	$5.4^{+2.2}_{-1.1}$	$\nu 5^2 \pi 5^1$	[23]
$^{86}\text{Zr}(4)$	$3.8^{+0.6}_{-0.5}$	$\nu 5^2 \pi 5^1$	[23]
$^{87}\text{Nb}(1)$	$5.2^{+1.1}_{-0.8}$	$\nu 5^3 \pi 5^1$	[24]
$^{87}\text{Nb}(2)$	$5.0^{+0.7}_{-1.0}$	$\nu 5^3 \pi 5^1$	[24]
$^{87}\text{Nb}(3)$	$5.3^{+1.2}_{-1.0}$	$\nu 5^3 \pi 5^1$	[24]
$^{88}\text{Mo}(1)$	$5.2^{+0.3}_{-0.3}$	$\nu 5^2 \pi 5^1 / \nu 5^2 \pi 5^0$	[8]
$^{88}\text{Mo}(2)$	$7.6^{+5.3}_{-1.7}$	$\nu 5^2 \pi 5^1$	[8]
$^{89}\text{Tc}(1)$	$5.9^{+0.7}_{-0.5}$	$\nu 5^2 \pi 5^1$	[8]
$^{91}\text{Tc}$	$6.7^{+1.3}_{-0.8}$	$\nu 5^3 \pi 5^2 / \nu 5^4 \pi 5^{2a}$	[13]

<sup>a</sup>These assignments assume a prolate shape.

Assuming that  $\beta_2$  and  $\gamma$  are the only deformation parameters that have nonzero values, that the moments of inertia of  $^{91}\text{Tc}$  and  $^{89}\text{Tc}$  deviate from that of a rigid body in a similar manner, and that the latter nucleus has close to axial deformation, a simple calculation with  $\beta_2 \approx 0.65$  and  $\gamma \approx 12^\circ$  reproduces the experimental values for  $\mathcal{J}^{(2)}$  and  $Q_t$ . The larger  $\mathcal{J}^{(2)}$  value may also be attributed to a smooth and gradual band crossing.

In order to interpret the experimental data on SD structures in the  $A \approx 80-90$  mass region, we have performed self-consistent mean field calculations based on a Woods-Saxon potential [16–20]. For  $^{91}\text{Tc}$  the calculations predict the presence of several SD configurations, associated with both triaxial and prolate shapes, near the Fermi level in the spin range where the SD band of  $^{91}\text{Tc}$  is fed. Therefore, it is difficult to make a definite configuration assignment for this SD band. It should also be noted that the  $Q_t$  value deduced from the experimental data only estimates the *average* transition quadrupole moment for all the states in the band, whereas the deformation may not stay constant throughout the entire sequence. The experimental  $\mathcal{J}^{(2)}$  curve exhibits a rise at the top of the band. One possible explanation for this feature may be the presence of a band crossing at the highest rotational frequencies.

#### A. Systematics of $Q_t$ values for SD bands in the mass region

Experimentally deduced transition quadrupole moments for the SD bands in the  $A \approx 80-90$  mass region and assigned occupation numbers for the  $\mathcal{N}=5$  intruder orbitals are given in Table II. The  $Q_t$  values, divided by  $ZA^{2/3}$  in order to remove the macroscopic  $A$  and  $Z$  dependencies, are plotted as a function of  $Z$  in Fig. 6. In the Woods-Saxon single-particle diagram of Fig. 7, the superdeformed shell gaps move towards larger deformations with increasing proton numbers (the trend is similar for the neutrons) for the nuclei in the  $A \approx 80-90$  mass region. A simple, approximate relation between the deformation parameter  $\beta_2$  and the quadrupole moment is given by [21]

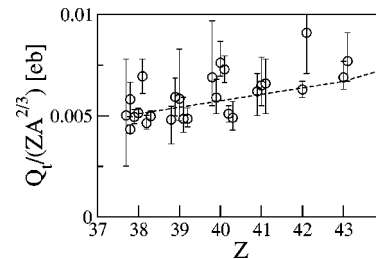


FIG. 6. Experimentally deduced transition quadrupole moments divided by  $ZA^{2/3}$  as a function of  $Z$  for the SD bands in the neutron-deficient  $A \approx 80-90$  mass region are shown with error bars. The data points have been offset slightly from the corresponding  $Z$  value for improved readability. The dashed line shows the quadrupole moment as defined by the simple relation 1, where  $\beta_2$  is taken as the predicted mean SD shell gap deformations (see, e.g., Fig 7). The tendency of a systematically increasing  $Q_t$  and  $\beta_2$  deformation as a function of  $Z$  present in the data is reproduced by the simple theoretical model.

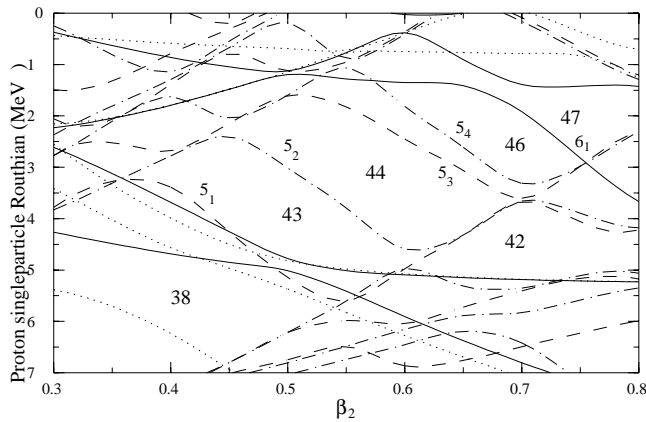


FIG. 7. Woods-Saxon single-proton diagram as a function of  $\beta_2$  deformation, valid for  $Z \approx 40$ , at a rotational frequency of  $\hbar\omega = 0.8$  MeV. Proton numbers for the largest shell gaps and intruder orbitals emanating from the  $N=5$  and 6 shells are indicated in the figure. The symbols for the different  $(\pi, \alpha)$  configurations: solid,  $(+, \frac{1}{2})$ ; dotted:  $(+, -\frac{1}{2})$ ; dash dotted:  $(-, \frac{1}{2})$ ; and dashed,  $(-, -\frac{1}{2})$ .

$$Q_t \approx \frac{3}{\sqrt{5\pi}} R^2 Z \beta_2 (1 + 0.16\beta_2). \quad (1)$$

The dashed line in Fig. 6 was obtained using this expression and the predicted shell gap deformations at different values of  $Z$ . The experimental trend of increasing  $Q_t$  with increasing  $Z$  is rather nicely reproduced by the simple model calculation.

## V. CONCLUSIONS

The previously reported SD bands in  $^{88}\text{Mo}$ ,  $^{89}\text{Tc}$ , and  $^{91}\text{Tc}$  were studied experimentally. Transition quadrupole moments, with a significantly improved experimental accuracy, were deduced for the strongest bands. The dynamical moment of inertia of the superdeformed band assigned to  $^{91}\text{Tc}$  is significantly higher than that for the bands in the other nuclei, which may indicate that it has a larger deformation. However, the transition quadrupole moment deduced from the present experiment is lower than can be expected for a purely prolate nucleus with such high  $\mathcal{J}^{(2)}$  values. The presence of a smooth and gradual band crossing and a triaxial shape of the SD band in  $^{91}\text{Tc}$  are two possible explanations for this.

A gradual increase in  $\beta_2$  deformation as a function of  $N$  and  $Z$  for SD states in the neutron-deficient mass 80–90 region has been predicted by shell model calculations and was confirmed in a systematic study of experimentally deduced transition quadrupole moments for SD bands in this mass region.

## ACKNOWLEDGMENTS

The authors would like to thank John Greene for providing targets. This work was supported by the Swedish Research Council and by the U.S. Department of Energy through Contract Nos. W-31-109-ENG-38 (ANL), DE-FG05-88ER40406 (Washington University), and DE-AC03-76SF00093 (LBNL).

- 
- [1] C. Baktash *et al.*, Phys. Rev. Lett. **74**, 1946 (1995).
  - [2] K. Lagergren *et al.* (unpublished).
  - [3] I.-Y. Lee, Nucl. Phys. **A520**, 641c (1990).
  - [4] M. Devlin *et al.*, Nucl. Instrum. Methods Phys. Res. A **383**, 506 (1996).
  - [5] C. Svensson *et al.*, Nucl. Instrum. Methods Phys. Res. A **396**, 228 (1997); **403**, 57(E) (1998).
  - [6] D. G. Sarantites *et al.*, Nucl. Instrum. Methods Phys. Res. A **381**, 418 (1996).
  - [7] M. Weiszflog *et al.*, Z. Phys. A **342**, 257 (1992).
  - [8] K. Lagergren *et al.* (unpublished).
  - [9] B. Cederwall *et al.*, Nucl. Instrum. Methods Phys. Res. A **354**, 591 (1995).
  - [10] J. F. Ziegler, J. P. Biersack, and U. Littmark, *The Stopping and Ranges of Ions in Matter* (Pergamon, London, 1985), Vol. 1.
  - [11] T. Bäck *et al.*, Eur. Phys. J. A **6**, 391 (1999).
  - [12] B. Cederwall *et al.*, Eur. Phys. J. A **6**, 251 (1999).
  - [13] E. Ideguchi *et al.*, Phys. Lett. B **492**, 245 (2000).
  - [14] D. Rudolph *et al.*, Nucl. Phys. **A587**, 181 (1995).
  - [15] D. Rudolph *et al.*, Phys. Rev. C **49**, 66 (1994).
  - [16] W. Nazarewicz, R. Wyss, and A. Johnson, Nucl. Phys. **A503**, 285 (1989).
  - [17] S. Ćwiok *et al.*, Comput. Phys. Commun. **46**, 379 (1987).
  - [18] W. Satula and R. Wyss, Phys. Scr. **T56**, 159 (1995).
  - [19] R. Wyss, W. Satula, and P. Magierski, Nucl. Phys. **A578**, 45 (1994).
  - [20] H. C. Pradhan, Y. Nogami, and J. Law, Nucl. Phys. **A201**, 357 (1973).
  - [21] Aage Bohr and Ben R. Mottelson, *Nuclear Structure, Nuclear Deformations* Vol. II (World Scientific Singapore, 1998).
  - [22] F. Lerma *et al.*, Phys. Rev. C **67**, 044310 (2003).
  - [23] D. G. Sarantites *et al.*, Phys. Rev. C **57**, R1 (1998).
  - [24] D. R. LaFosse *et al.*, Phys. Rev. Lett. **78**, 614 (1997).